Particle Tracking with Scintillating Fibers

C. D'Ambrosio, T. Gys, H. Leutz, and D. Puertolas

***Abstract*—This paper presents our research and development work on particle tracking with scintillating fibers. We have developed new fiber dyes, more efficient fiber cladding, coherent fiber bundles with improved packing fraction, and a new fiber readout technique (ISPA-tube). Altogether, these new developments increased the hit density of fine grain (60 μm) fibers by about seven times. This results in mini-tracks per 2.5-mm fiber layer rather than in single hits only and enhances the track reconstruction efficiency to nearly 100%. Compared with competing tracking methods (silicon strips, micro strip gas chambers), our scintillating fibers are superior in hit numbers per radiation length and in the two-track resolution. They require much less readout channels and consequently no cooling provisions to remove their electronic heat.**

I. Introduction

THE LARGE Hadron Collider (LHC) at CERN will be equipped with two multipurpose detectors, CMS [1] and ATLAS [2], at its interaction points 1 and 5, respectively. Both systems will provide particle tracking within their central cylindrical cavities. These will be enclosed by either the inner surface of an electromagnetic calorimeter at 1.3-m inner radius (CMS) or by the vacuum vessel of the cryostat for a solenoid coil and for a liquid argon calorimeter at 1.15-m inner radius (ATLAS). Solenoids of 4 T (CMS) or 2 T (ATLAS) flux densities will fill the tracking cavities of 6-m (CMS) or 5.3-m length (ATLAS) with magnetic field lines parallel to the collider axis.

The proposed particle tracking is based on silicon (or GaAs) pixels arranged close to the interaction points of both detectors and, in the large cavity volume, on silicon strips interleaved with transition radiation detectors (TRD's) in ATLAS or on additional micro strip gas chambers (MSGC's) in CMS. The intention of this article is to present our recent research and development activities and to remind people of a further alternative for large-volume tracking, namely with scintillating fibers. An example for such a tracking arrangement is shown in Fig. 1 (radial-azimuth view) and Fig. 2 (radial-polar view). It consists of three thin-fiber shells, each composed of parallel (φ) and stereo (u, v) layers. Their scintillation signals are read out with imaging silicon pixel array (ISPA) tubes [3] attached to the end-sections of each half shell at approximately 90° polar angle.

To demonstrate the power and reliability of our fiber tracker, we first list the most essential tracking parameters. Then, we verify each of them with respect to the measured results achieved with our scintillating fibers. Finally, we compare the relevant parameters of our fiber tracker with those quoted for silicon strip and MSGC tracking.

Manuscript received November 21, 1995; revised February 27, 1996.
The authors are with CERN, Geneva, Switzerland.
Publisher Item Identifier S 0018-9499(96)04850-2.

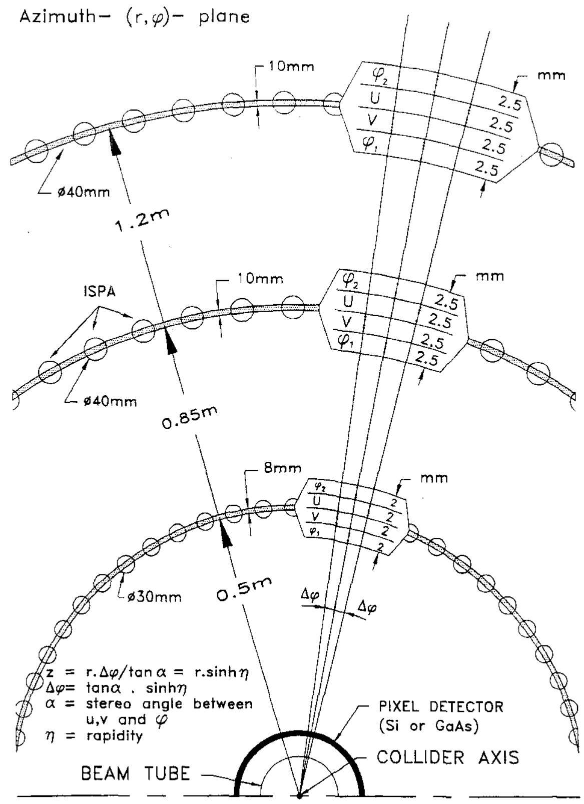

Fig. 1. Radial-azimuthal arrangement of fiber shells for tracking in the central barrel region of an LHC detector. The magnified parts show the shell subdivision into straight (φ) and oblique (u, v) layers. The symmetric angles $\Delta\varphi$ indicate the z-coordinate via the indicated relations. The radial distances of the three shells apply to CMS and would change to 0.4, 0.75, and 1.10 m for ATLAS.

II. Design Considerations for Particle Tracking

Successful tracking within the central cavity of an LHC detector means reconstructing charged particles of large transverse momentum with high efficiency and excellent momentum resolution. This requires high detection efficiency per unit of radiation length of the tracker elements. In addition, efficient track finding and reconstruction requires excellent two-track resolution. Moreover, the obtained momentum resolution should at least match the energy resolution of the hadron calorimeter.

These requirements imply low occupancies of tracker elements to eliminate dead time or pile-up, which would reduce

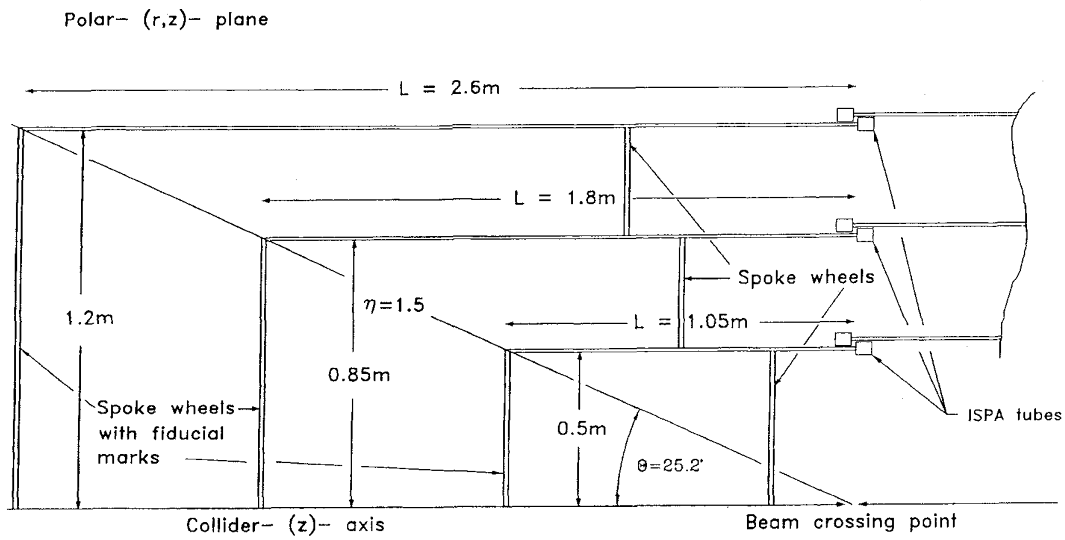

Fig. 2. Radial–polar arrangement of fiber shells. At 90° polar angle they are divided into half shells with ISPA tubes for the readout of fiber signals. The shells are kept in radial position by thin-walled (5 mm) plexiglass spoke wheels.

the detection efficiency. Also, confusion with ghost tracks should be avoided by choosing tracker materials of long radiation length, which helps to reduce secondary interactions and γ conversions. This includes the support structures for the active tracker elements.

To avoid frequent recalibration of the particle tracker or even replacement of its elements, their radiation hardness should be sufficient to tolerate several years of collider operation. This radiation resistance should be achieved at ambient temperature since any refrigeration could moisten the tracking elements and provoke malfunctions.

The number of electronic readout channels should be kept small. This reduces the complexity of front-end electronics and facilitates the data transfer to their acquisition facilities outside the detector. An important issue is the heat production of these electronic channels. If it increases the detector temperature, it has to be removed by complicated cooling systems.

The alignment of the tracker elements should be guaranteed within a few μm. It should be possible to check them on-line during collider runs to verify their correct positions.

III. Realization of the Design Considerations

A. Detection Efficiency

The detected number of photoelectrons per mm fiber layer (hit density) for the passage of minimum ionizing particles is plotted in Fig. 3. The two lower curves are measured with particles of normal incidence to the fiber bundles without [4] and with [5] mirrored end face opposite to a hybrid photomultiplier tube (HPMT) [6]. The three upper curves are calculated from curve 2 according to the particle paths resulting from varying polar angles of incidence at the three fiber shells.

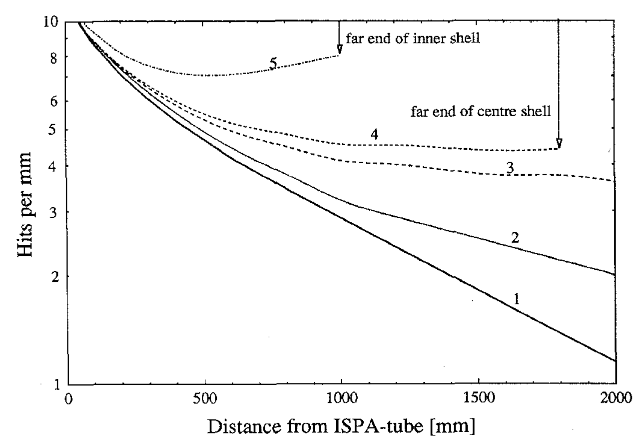

Fig. 3. Hit densities (number of photoelectrons per mm fiber thickness d) of fiber bundles containing 60-μm individual fibers (Figs. 4 and 5) without (curve 1) and with mirrored end face (curve 2). The three upper curves indicate the hit densities arising from changing polar angles θ (Fig. 2) for the outer (curve 3), center (curve 4), and inner (curve 5) fiber shells (hit density = hits/$d \sin \theta$).

The comparatively high hit densities in Fig. 3 result from a series of recent developments.

1) The light trapping fraction (total reflections) in the fibers has been increased by 1.8 times with the application of fluorinated methacrylate cladding [7], [8] of 1.42 refractive index.
2) The packing fraction (ratio of effective to total fiber cross section) has been improved by applying fused fiber bundles [9] (Fig. 4) where the hexagonal-shaped individual fibers share their cladding with their next neighbors (Fig. 5), from 0.67 for circular-shaped fibers to 0.85 for hexagonal ones (1.3 times) (Fig. 6).
3) The usual doping of plastic scintillators with p-terphenyl and an additional wavelength shifter (two-component system) has been replaced by a one-component dye

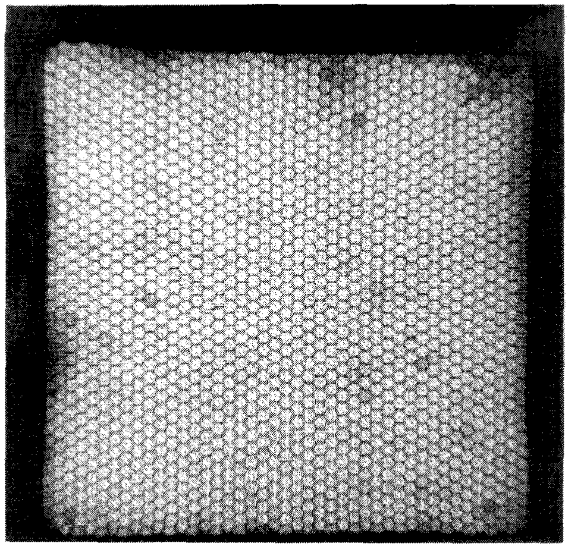

Fig. 4. Fiber bundle of 2.5-mm edge lengths. It contains about 1600 individual fibers of hexagonal shape and 60-μm "diameter." The photograph is taken with a CCD camera through 2 m of bundle length [9].

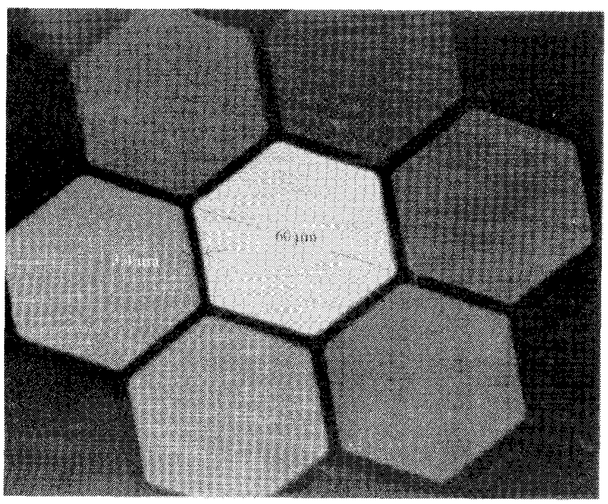

Fig. 5. An individual fiber within the bundle of Fig. 4 surrounded by its six next neighbors. The picture was taken through a microscope objective according to the arrangement of [9].

(PMP).[1] Due to its large Stokes shift, this dye emits directly in the visible spectral region. In this way, it avoids self-absorption of its emitted light due to the overlap of absorption- and emission-bands. At the same time any cross-talk is avoided. The new dye improved the light output about 1.8 times.

4) The large potential difference between photocathode and silicon anode of the HPMT (the same holds for the ISPA-tube) enhances by 1.6 times the photoelectron collection efficiency as compared to a photomultiplier.

[1]Together with collaborators from other institutions (Forschungszentrum Karlsruhe, Germany; CNRS, Toulouse, France; University of Torino, Italy) we successfully synthesized other one-component dyes. Their performances in Stokes shifts and light emission will be reported in a separate paper.

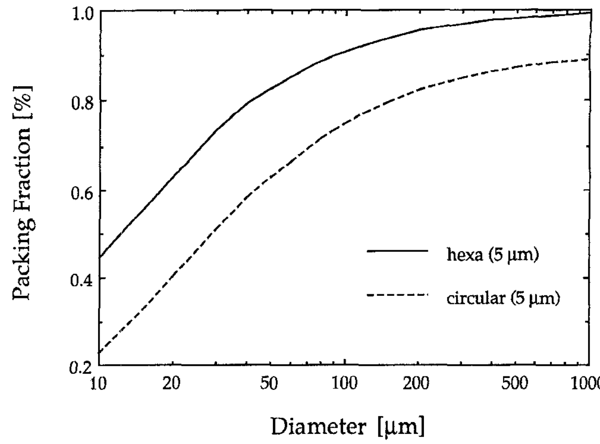

Fig. 6. Packing fractions (ratios of scintillating to total cross sections) of hexagonal-shaped fibers and circular capillaries with their respective cladding layers.

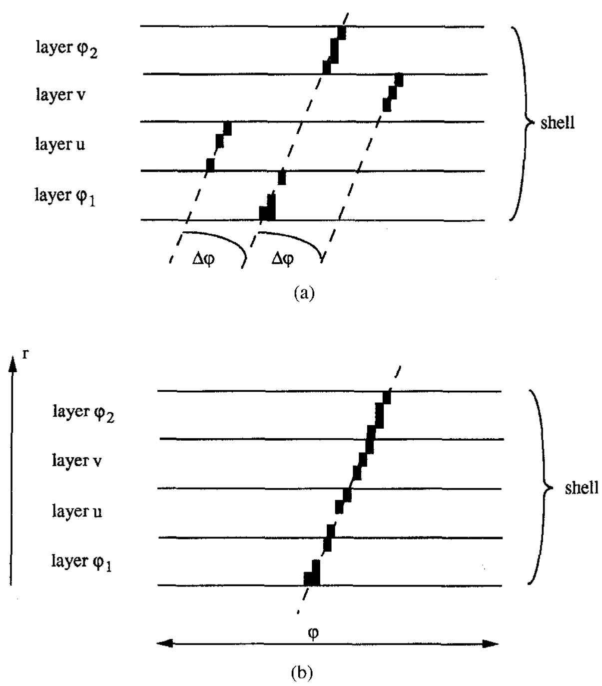

Fig. 7. (a) Mini-track triplet from a particle passing a tracker shell of radius r at $z = \Delta\varphi r/\sin\alpha$ and seen at the end-section by an ISPA-tube. The u and v tracks are shifted symmetrically with respect to the φ_1 and φ_2 tracks. α means the stereo angle between u, v and φ. (b) The resulting shell-track after shifting the u and v tracks by $\pm\Delta\varphi = \pm\tan\alpha\sinh\eta$.

B. Track Finding and Reconstruction

For this procedure we developed [10] an algorithm with specific application to a fiber tracker. It is based on the fact that each fiber layer exhibits, due to its high hit density, mini-tracks rather than points only. These mini-tracks provide already track directions and indicate therefore precise search roads to extend them to subsequent fiber layers. According to this strategy, we start with mini-tracks in the φ_2-layer of the outermost fiber shell and search for all mini-tracks fitting to them in the φ_1-layer. Then, we look in the u and v layers for

TABLE I
PROPERTIES OF POLYSTYRENE, THE CORE MATERIAL OF OUR FIBERS

General properties		
Chemical formula :	$(C_6H_5CH{:}CH_2)_n$	
Molecular weight	g mole^{-1}	104.15
Density	g cm^{-3}	1.03
Number of atoms	cm^{-3}	$1\text{x}10^{23}$
Proton / Neutron ratio		1.17
Melting point	°C	240
Thermal conductivity	W cm^{-1} K^{-1}	0.105
Linear thermal expansion coefficient	K^{-1}	$7\text{x}10^{5}$
Tensile modulus (E)	MPa	3200
Dielectric constant		2.5
Optical properties		
Refractive index		1.59 (590 nm)
		1.58 (480 nm)
Optical dispersion	ns m^{-1}	0.04 (400 nm to 500 nm)
Light decay (1/e)	ns	2 to 3 (depending on dopant)
Light velocity in PS	m ns^{-1}	0.21
Numerical aperture		0.53 (n cladding = 1.49)
		0.69 (n cladding = 1.42)
Photon yield (with dopant)	(keV)$^{-1}$	~10 (depending on dopant)
Absorption peak	nm	265
Emission peak	nm	330
Fluorescence Yield		0.03
Radiation properties		
Radiation length	cm	42.4
Gamma conversion length	cm	54.5
Nuclear interaction length	cm	79.6
Multiple scattering angle	µrad	50 (10 GeV/c; 1 mmPS)
(dE/dx) min.	MeV cm^{-1}	2.0

mini-tracks being symmetric to those in the φ_1 and φ_2 layers. They form u, v, φ triplets and their symmetric distances $\Delta\varphi$ (Fig. 7) indicate, together with the stereo angle α of the fiber layers and the radial distance r, the z-coordinate of the particle track

$$z = \frac{\Delta\varphi r}{\tan\alpha}. \tag{1}$$

To extend the mini-tracks from the outer shell to the center one, we shift all u and v tracks to their symmetry axes φ_1 and φ_2 to obtain $\sim$10-mm-long track segments. They point with an angular precision of about 8 mrad [Fig. 15(c)] to the center shell. Here, we repeat the same procedure employed in the outer shell already and then proceed to the inner one.

We applied this track-finding algorithm to Monte Carlo-generated e^+e^- collisions [10]. The hits of their charged particles were simulated in the two shells of a fiber tracker placed in the inner barrel volume of the L3 detector at LEP. After this procedure, we searched for and reconstructed tracks as explained above. With two fiber shells only, the reconstruction efficiency was close to 100% with less than 1% ghost tracks. This excellent result is mainly due to the high hit density (Fig. 3) and the fine granularity of the fibers.

C. Momentum Resolution

The momentum resolution $\frac{\Delta p}{p}$ is composed of a transverse component (index t), which indicates the track curvature projected into the (r, φ) plane (Fig. 1), and of a longitudinal one (index //) showing the slope of the track in the (r, z) plane (Fig. 2) where the projected tracks are straight for particle momenta >10 GeV/c at $B = 3.3$ T

$$\begin{aligned}\left(\frac{\delta p}{p}\right)^2 = &\left\{\left(\frac{G_c}{N}\right)^{1/2} \times \left(\frac{\sigma}{L^2}\right) \times \left(\frac{p\sin\theta}{0.3B}\right)\right\}^2_{\text{curv.}} \\ &+ \left\{t^{1/2} \times \left(\frac{0.016\sin\theta}{0.3BL}\right)\right\}^2_{\text{mult.sc.}}\Bigg\}p_t \\ &+ \left\{\left(\frac{G_{\text{sl}}}{N}\right)^{1/2} \times \left(\frac{\sigma\cos\theta}{L\sin\alpha}\right)\right\}^2_{\text{slope}} \\ &+ \left\{\left(\frac{t}{\sin\theta}\right)^{1/2} \times \left(\frac{0.014}{p\,\text{tg}\theta}\right)\right\}^2_{\text{mult.sc.}}\Bigg\}p_{//}.\end{aligned} \tag{2}$$

σ [m] is the spatial precision, L [m] is the distance between the collider axis and the outermost shell, B [T] is the magnetic flux density, t is the tracker material layer in units of radiation lengths, (X_0), N is the number of hits along the track, G_c

TABLE II
COMPARISON OF RADIATION LENGTHS X_0 SEEN IN THE TRACKING VOLUME BY PARTICLES EMITTED AT DIFFERENT RAPIDITIES η (POLAR ANGLES θ) FOR THE PROPOSED TRACKING ARRANGEMENTS

η	θ degrees	ATLAS [2] % X0	CMS [1] % X0	Fibre tracker % X0
0	90	18.5	12.0	8.0
0.5	62.4	(33.5)	30.0	9.0
1.0	40.4	48.5	40.0	12.0
1.5	25.2	(48.0)	60.0	19.0

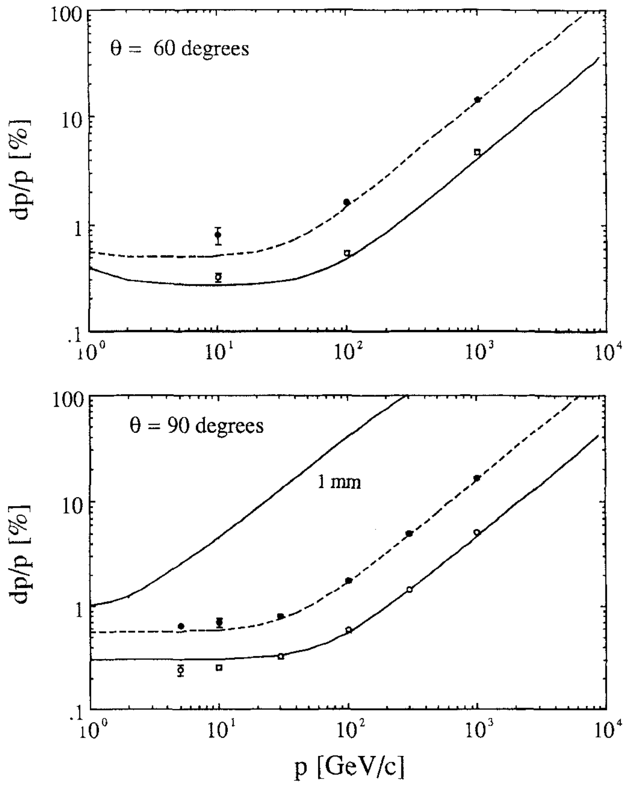

Fig. 8. Momentum resolution for particle tracks produced at different polar angles θ. The curves are obtained from (2) for 60-μm hexagonal fibers. The points result from Monte–Carlo simulations [14]. Open (full) points and solid (dashed) curves are results with (without) beam constraints. For fibers of 1 mm diameter the momentum resolution increases by 16.6 times.

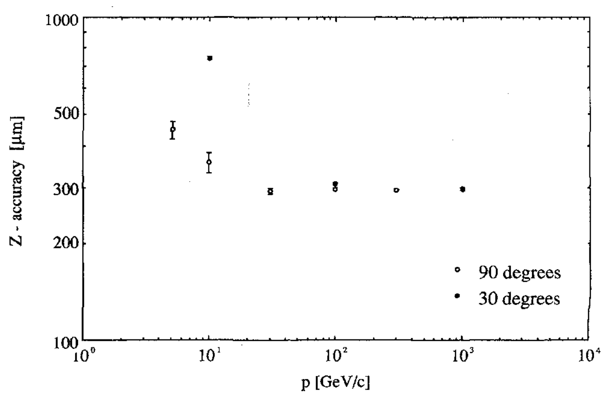

Fig. 9. z accuracy versus track momentum for 90° polar angle.

is a number that varies between 256 for optimum hit spacing (hits at both ends and in the middle of a track) and 720 for continuous hit distribution along the track, and, finally, G_{sl}, which varies in the same way between 2 and 10 [11]. Our shell arrangement (Fig. 1) matches nearly the optimum hit spacing.

The momentum resolution for the tracker configuration of Figs. 1 and 2 has been calculated [12] on the basis of the measured parameters σ (30 μm [9], [13]), the hit number N, the track length L (1.25 m, which includes the beam position as a constraint) and the material thickness t ($0.09X_o$). This calculation has been checked by a Monte Carlo study [14] that used GEANT [15] to trace charged particles through the tracker configuration of Figs. 1 and 2. The tracks were reconstructed with the Kalman filtering method [16]. Some results are displayed for 90° and 60° polar angle in Fig. 8 and for the z resolution in Fig. 9. These momentum resolutions would be ~20 times worse if fibers of 1 mm diameter would be employed.

D. Occupancy

Occupancy means the fraction of tracker elements occupied by particle hits between two bunch crossings. This fraction O is proportional to the collider's luminosity L (10^{34} cm^{-2}s^{-1}, which contains the bunch collision frequency $(1/t_b)$), the cross-section σ (85 mb) of the colliding protons, the number n (6) of minimum bias particles produced per bunch crossing and per unit of rapidity η, and the time t_b (25 ns) between two bunch crossings. It also takes into account the following tracker parameters: radial distance r (50, 85, 120 cm), the transverse dimension s of a tracker element (0.006 cm) and the rapidity $\eta_{\max}$ covered by the inner tracker

$$O = (L\sigma n t_b) \times \left(\frac{s\eta_{\max}}{2\pi r}\right). \tag{3}$$

As soon as the element busy time t exceeds the bunch crossing time t_b (e.g., in MSGC's), then t_b has to be replaced by t.

The first bracket in (3) has a value of 127.5 and for the second one we obtain 2.9×10^{-5}, 1.7×10^{-5}, and 1.2×10^{-5} and therefore occupancies of 0.36% for the fibers in the inner shell, 0.21% for those in the center shell, and 0.15% for those in the outer shell of our fiber tracker. With fibers of 1 mm

TABLE III
COMPARISON OF RELEVANT PARAMETERS BETWEEN DIFFERENT TRACKING DETECTORS. X_0 MEANS THE RADIATION LENGTH AND H THE MATERIAL LAYER THICKNESS REQUIRED TO ACHIEVE ONE HIT OR CLUSTER (Si: 0.3 mm, MSGC: 2 mm, fibers: 0.25 mm)

Parameters	Si strips	MSGCs	Fibres
Number of hits $[(0.1\ X_0)^{-1}]$	15-30 [a]	~10-15 [b]	84-250 [c]
Cell busy time [ns]	<15	~50	<15
Intrinsic spatial resolution [μm]	5-14 [d]	40 [e]	15-40 [f]
Two track resolution [μm]	100	250 [e]	47-94 [f]
Angular resolution [mrad]	none	none	10 [f]
Occupancy (10^{34} cm^{-2} s^{-1} luminosity) [%]	<1	2-3	<1
Number of readout channels $[m^{-2}\ H^{-1}]$	$2x10^5$ [g]	$5x10^4$ [h]	$4x10^3$ [i]
Heat production $[W\ m^{-2}\ H^{-1}]$	100 [j]	25 [j]	0.4 [k]

[a] (0.3 mm detector + 0.3 mm electronic layer) per hit; higher number without electronics.
[b] F. Angelini et al., CERN-PPE 91-122.
[c] 2 (6) hit(s) per mm at 2 m (0.35 m); bundles with mirrored end face (fig. 3).
[d] Silicon strips with 20 or 50 μm pitch, divided by √12.
[e] MSGC with 200 μm pitch, taking the centroid [34].
[f] Measurements [9, 13, 23] with 60 μm diameter fibres.
[g] Silicon strip of 50 μm pitch and 10 cm length.
[h] Microstrip gas counter of 200 μm and 10 cm length.
[i] Each pixel channel of an ISPA tube covers 0.5 x 0.05 = 0.025 mm^2 fibre endsection. This corresponds to a subtended detector surface of : 0.025 mm^2 x 2.5 m (fibre length) / 0.25 mm = $2.5x10^{-4}$ m^2.
[j] Assuming 0.5 mW per channel.
[k] Assuming 0.1 mW per channel.

diameter, we would obtain 6% occupancy in the inner shell. This confirms our choice of fiber diameters below 0.1 mm.[2]

E. Production of Secondaries, γ Conversions, and Noise in the Fiber Tracker

The hit number N of a particle track increases with the material layer thickness of the tracker elements. However, the fraction of unwanted secondary interactions, γ conversions, and multiple scattering processes increases with this layer thickness as well. Therefore, we carefully balanced these effects by optimizing the material layer thickness to keep the unwanted terms negligibly small while maintaining a hit number N high enough to produce clear and visible mini-tracks in the fiber layers φ, u, and v. The results of this balance are the layer thicknesses indicated in Fig. 1.

The excellent signal (hit number) to noise (unwanted effects) ratio achieved is due to high hit densities of our fiber bundles (Fig. 3) and to the comparatively long radiation length (resulting in 18-μrad multiple scattering angle per shell at 100 GeV), γ-conversion length (1.8% pair production per shell), and interaction length (1.2% hadronic interactions per shell) of polystyrene, the core-material of our fibers (Table I). This advantage of scintillating fibers becomes also obvious if we compare in Table II the fraction of radiation lengths seen by particles emitted at different rapidities for CMS [1], ATLAS [2], and scintillating fibers replacing the proposed tracking arrangements in both detectors, or the hit number per unit of length listed in the first line of Table III for the three tracking methods.

[2] 60-μm-diameter fibers produce 3% ghost tracks, however 1-mm-diameter fibers produce 50% ghost tracks (both with $\pm 4°$ stereo angle [12]).

Also, optical cross-talk between individual fibers within a fiber bundle is suppressed [Fig. 10(b)] since our fibers are doped with one dye only (PMP [17], [18]). This causes local energy transitions [19], [20] rather than radiative ones if wavelength shifters between the first and second dye are employed. In this case the energy transition is not local anymore because the reabsorption of the light emission from the first dye by the second one needs about 200-μm attenuation. This process provokes cross-talk between fibers of small diameter [Fig. 10(a)].

F. Radiation Levels in the Tracker Shells

Minimum-bias events produced from pp collisions contribute most to the radiation dose in the tracking cavity. They scale with the collider's luminosity L (10^{34} $\mathrm{cm^{-2}s^{-1}}$),[3] the particle multiplicity ($n = 6$ per collision and unit of rapidity), and with the inelastic collision cross-section ($\sigma = 85$ mb). All numbers are for LHC and the dose rate D_0 in Gy (1 Gy $=$ 1 $\mathrm{Jkg^{-1}}$ $=$ 100 Rad) per year (10^7 s assuming 115 days of yearly operation) can be expressed as

$$D_0(r) = 1.6 \times 10^{-3} \times (L\sigma n) \times \left(\frac{dE}{\sin\theta dx} \times \frac{\sin\theta}{2\pi r^2}\right) \quad (4)$$

with $(dE/dx)(\sin\theta)^{-1}$ meaning the stopping power (2 GeV $\mathrm{cm^2kg^{-1}}$) of minimum ionizing particles emitted at the polar angle θ (Fig. 2), $2\pi r$ the circumferences of a fiber shell, and $n\sin\theta/2\pi r^2$ the number of particles produced per collision and passing per unit surface of a fiber shell. The term $1.6 \times$

[3] L means the design luminosity after a LHC fill. The average luminosity $\langle L\rangle$ depends on the number of collision points and on the luminosity half life. Therefore, it is safe to assume $\langle L\rangle \approx 0.5L$.

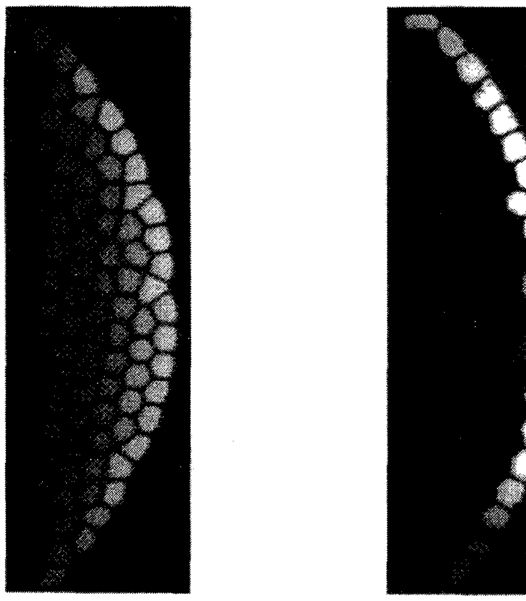

(a) (b)

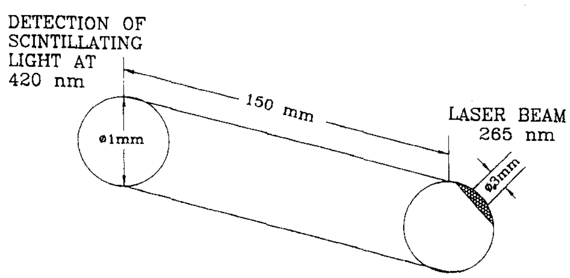

(c)

Fig. 10. Cross-talk of scintillating fibers. Two fiber bundles of 1 mm diameter, each containing about 850 individual fibers of 30 μm diameter, were excited at one bundle end by a 0.3-mm-diameter Nd-Yag laser beam of 265-nm wavelength: (a) The fibers doped with p terphenyl and an additional wavelength shifter show at their opposite bundle end cross-talk over several fibers layers. (b) The PMP-doped fibers show local energy (Förster [20]) transitions, and therefore no cross-talk, at their opposite bundle end. Their higher light output show that all scintillations stay in the absorbing first bundle layer. (c) Experimental arrangement.

10^{-3} (J $\text{GeV}^{-1}\text{Yr}^{-1}$) contains the conversions into Joules (1.6×10^{-10}) and years (10^7).

With a solenoidal field of magnetic flux density B (T) the annual dose D_0 of (4) changes to

$$D_B(r) = D_0(r)\left(2\langle n_c\rangle \int_{X_i}^{X_b} f(x')dx' + \int_{X_b}^{\infty} f(x')dx'\right) \tag{5}$$

where $\langle n_c\rangle = \sinh \eta_{\max}/\pi \sinh \eta$ [12] is the average number of particle curls within the rapidity range $0 < \eta < \eta_{\max}$ of the tracker and $f(x) = xe^{-x}$ is the transverse momentum distribution of minimum bias particles with $x = 2p_t/\langle p_t\rangle = 0.3$ $\text{Br}/\langle p_t\rangle$. The average transverse momentum $\langle p_t\rangle$ is estimated to be ~530 MeV/c.

The first integral spans between the helix diameters ($d = p_t/0.15$ B [13]) of curling particles touching the inner fiber shell (X_i) and those reaching the inner calorimeter surface (X_b) bordering the tracker cavity.[4] The second integral covers the short track lengths of those particles that are absorbed by the calorimeter.

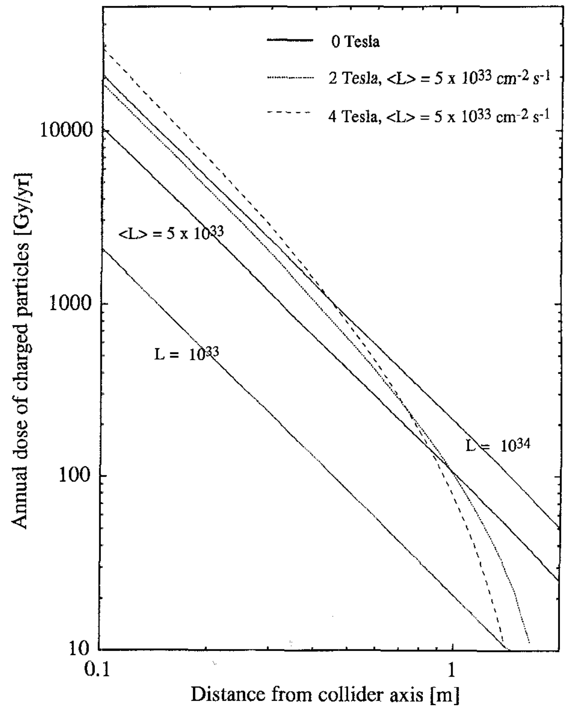

Fig. 11. Annual radiation doses versus distance from the collider axis within ± 1.5 rapidity. The indicated decadic luminosities show D_0 (relation 4) without solenoidal field. The doses D_B (relation 5) are for an average luminosity $\langle L\rangle = 5 \times 10^{33}$ $\text{cm}^{-2}\text{s}^{-1}$ and for magnetic flux densities of 2 T (ATLAS) and 4 T (CMS). The unit Gray (Gy) = 100 Rad and means 1 Joule/kg.

The annual doses D_0 for two LHC-filling luminosities (10^{33} and 10^{34} $\text{cm}^{-2}\text{s}^{-1}$) and for an average luminosity $\langle L\rangle$ (5×10^{33} $\text{cm}^{-2}\text{s}^{-1}$) are displayed versus the distance from the collider axis in Fig. 11. In addition, the doses D_B based on the average luminosity (5×10^{33} $\text{cm}^{-2}\text{s}^{-1}$) and magnetic flux densities of 2 T (ATLAS) and 4 T (CMS) in the tracking cavity are also plotted. The inner shell of our tracker receives the greatest annual dose D_B of 750 Gy (CMS) and 1000 Gy (ATLAS). To these values we must add the albedo neutron flux emerging mostly from the calorimeter. This flux over 1.5 units of rapidity covered by the tracker amounts to 2×10^{12} ($\text{cm}^{-2}\text{Yr}^{-1}$) neutrons [21]. Assuming 1-MeV neutron energy, we obtain for the neutron absorption in the inner fiber shell an annual neutron dose of 100 Gy at the average luminosity $\langle L\rangle$.[5] The total annual doses between 850 Gy and 1100 Gy are

[4] For particles emitted at large polar angles θ, the number of helix turns would become numerous or even infinite ($\theta = 90°$). This is avoided by particle decays. The polar emission angle θ_d above which the curling particles decay inside the tracker ($\eta_{\max}$) is $\text{cotg}\theta_d = \frac{m_0}{c\tau} \times \frac{\sinh \eta_{\max}}{0.15B}$ [13]. For charged pions ($m_0 = 0.14$ GeV/c^2, $c\tau = 7.8$ m) that constitute the vast majority of minimum bias particles, we obtain minimum polar angles θ_d between 76 and 27° for B between 1 T and 6 T and $\eta_{\max} = 1.5$.

[5] From the neutron cross sections of 4.6 barn (H) and 2.6 barn (C) at 1-MeV neutron, energy we obtain 0.34 cm^{-1} neutron absorption coefficient in polystyrene. This results, for 2×10^{12} $\text{cm}^{-2}\text{Yr}^{-1}$ neutron flux, in an absorbed neutron energy of about 5×10^{11} $\text{MeVcm}^{-2}\text{Yr}^{-1}$. This gives finally 100 $\text{Jkg}^{-1}\text{Yr}^{-1}$ or 100 GyYr^{-1}.

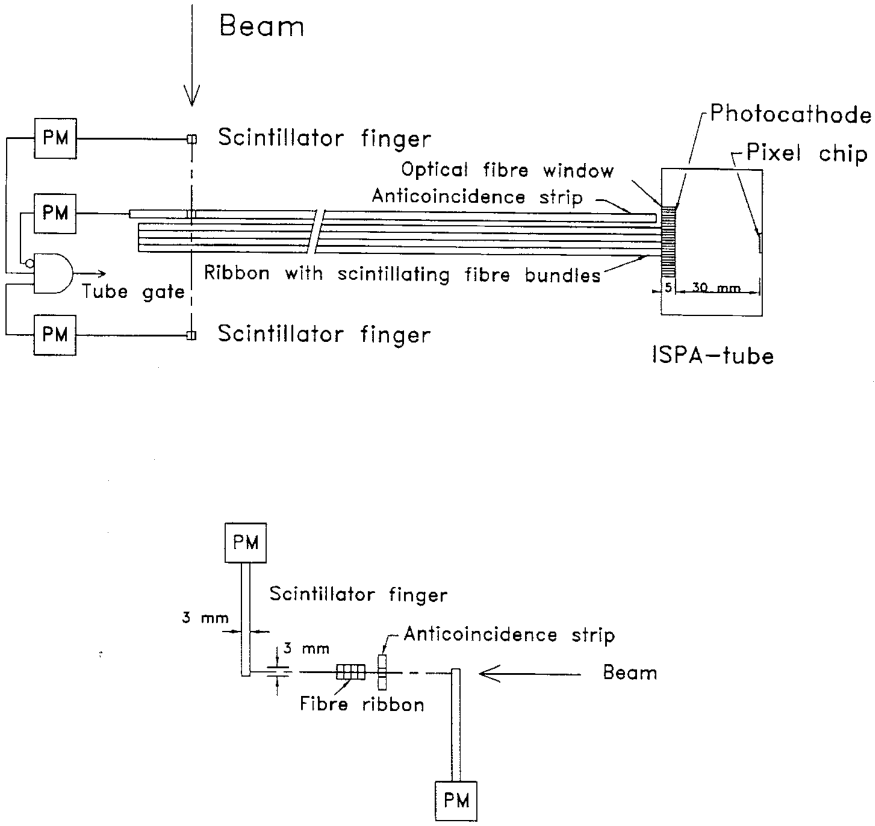

Fig. 12. Experimental layout of the 120-GeV/c pion beam exposure. The fiber ribbon is attached to the ISPA tube and consists of 2 × 4 fiber bundles, each containing about 1600 individual fibers of 60-μm transverse dimension. The pions traverse four fiber bundles (10 mm), two scintillating fingers wired in coincidence, and a 3-mm-diameter hole in the anticoincidence strip to select beam particles only.

certainly not harming the tracker performance during several years of operation [22].

G. Electronic Readout Channels and their Heat Production

A striking difference between our fiber tracker and those based on Si-strips and MSGC's (see Table III) is in their electronic readout. Fibers are readout at the end-sections of their shell arrangements (Fig. 2) via optoelectronic ISPA-tubes [3], [23]. They represent vacuum-sealed cylinders of about 20 mm length with diameters ranging between 30 and 80 mm. Photocathodes, evaporated onto the inner surface of an optical fiber window for collimated light passage, are viewed at proximity distances by 300-μm-thick detector chips of high-resistivity n-type silicon. They contain several thousands of rectangular pixels with 50-μm (azimuth coordinate) and 500-μm (radial coordinate) edges. Each of these detector pixels is bump-bonded to an equally sized front-end electronic pixel comprised of a preamplifier, comparator with adjustable threshold, delay line, coincidence logic, and memory element [24], [25]. The line-parallel readout of these pixels reduces their total readout time to less than 10 μs, and the connections leading through the vacuum-sealed envelope are only 2% compared to the number of detector pixels inside the tube. Each photoelectron hitting a detector pixel creates 280 electron-hole pairs per keV. With about 25-kV potential difference between photocathode and chip anode, the number of electron-hole pairs amounts to 7000, which is nearly three orders of magnitude higher than the electron multiplication at the first dynode of a photomultiplier. This high number of electron-hole pairs along with the Fano factor for silicon (0.1) provide extremely small statistical fluctuations.

Imaging silicon pixel array tubes considerably improve the time and spatial resolution and shorten readout times by more than two orders of magnitude compared with the usually adopted bulky optoelectronic chains consisting of three to four image intensifiers with a CCD-camera at the end for the readout [19], [26], [27]. The signals of each image intensifier within such a bulky chain are transported via phosphor screens to the subsequent photocathodes, which causes optical noise and losses in time and spatial resolution. In contrast, the ISPA tube is a one-stage light detector aligned parallel to the LHC detectors magnetic field, which conserves the spatial resolution of scintillating fibers by magnetic focussing of its photoelectrons.[6]

Another technique has been developed to readout large diameter scintillating fibers, the visible light photon counter (VLPC) [28], [29]. Its maximum photon sensitivity is around 550-nm wavelength. In order to reduce its dark current to photoelectron levels, it must be operated at 6.5 K. Therefore,

[6] Photoelectrons emitted from the photocathode with mv_t (eV/c) transverse momentum follow the magnetic field with a helix of $2mv_t/B = 17.5$ μm diameter at 1-T flux density B and 2.6-eV kinetic emission energy.

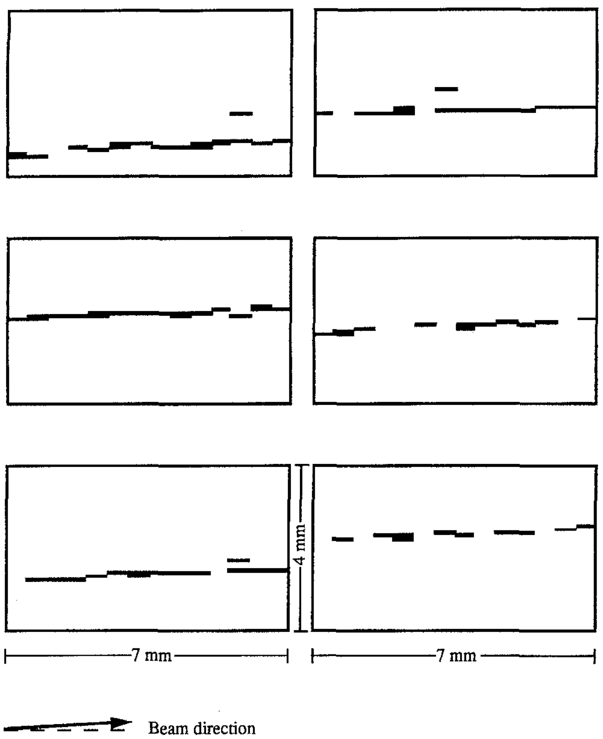

Fig. 13. Typical track patterns read out by the ISPA tube during the 120-GeV/c pion exposure. The pixel size is 75 μm $\times$ 500 μm (along the beam). Occasional hits aside the tracks are attributed to δ rays. Note that the beam was not exactly parallel to the pixel edges.

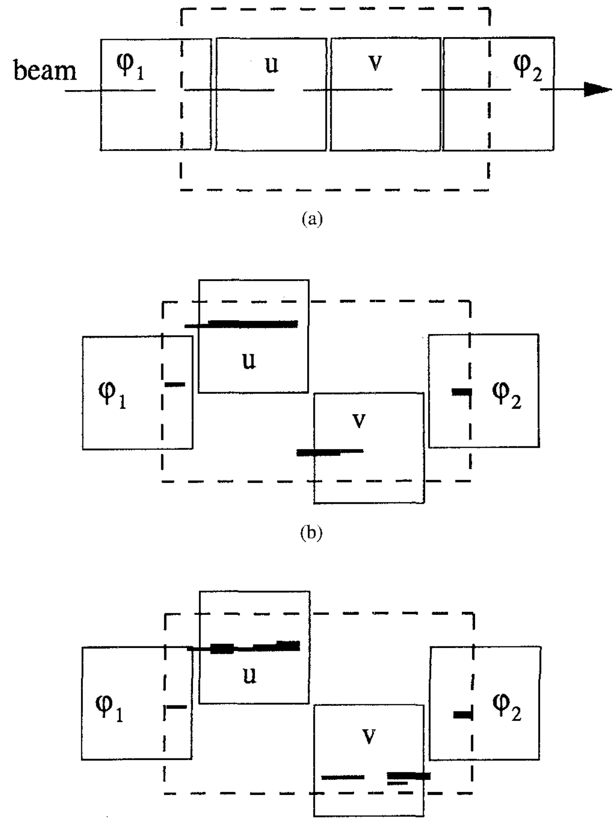

Fig. 14. Track patterns obtained with a stereoscopic bundle arrangement. (a) The beam passes straight through all four bundles. (b), (c) The bundles u and v run with a stereo angle $\pm\alpha = 7$ mrad oblique to the bundles φ_1 and φ_2. Therefore, the ISPA tube displays the track patterns (b) and (c) at a distance $z = (u+v)/2 \tan\alpha$ from the beam. The active frame of the ISPA anode chip (dashed area) only partly covers, with 7 mm length, the four bundles (10 mm). The stereo angle α was ten times smaller than foreseen for a fiber tracker.

clear fibers transmit the scintillating light to a dewar outside the detector. A study for a preshower detector [30] describes 1-m-long scintillating strips with 4.5 mm $\times$ 5 mm cross section and 1.5-m-long axial wavelength shifting double clad fibers (0.835 mm diameter) doped with 1% p terphenyl and 1500 ppm 3-HF and coupled to 8-m-long clear fibers for a VLPC readout. Whereas the ISPA tube represents a fine grain light detector, VLPC's read out each fiber individually, which restricts the number of fibers and hence their diameter in a particle detector. This has consequences for the momentum resolution (Fig. 8) and the occupancy [see (3)]. Rise times of ISPA pixels and VLPC direct response are similar (<10 ns).

Beam tests with an ISPA tube closely attached with its photocathode to the end-sections of eight fiber bundles have been performed by tracking 120-GeV/c pions transversally through their 60-μm individual fibers [23]. The layout of this beam test is shown in Fig. 12. Typical track patterns are displayed in Fig. 13 and clearly show the expected mini-tracks. The ISPA pixels are oriented with their 500-μm edges almost parallel to the beam. In the tracker arrangement (Fig. 1) the 500-μm edges will be oriented radially to allow for optimum azimuthal resolution with the short pixel edges. Another bundle arrangement with bundles u- and v-oriented oblique to the parallel φ_1 and φ_2 ones is shown together with the corresponding mini-tracks in Fig. 14.

The transverse hit distribution in Fig. 15(a) shows a residual standard deviation of 42 μm, resulting in 100-μm full width at half maximum (FWHM) two-track resolution. These values would be reduced to 32 μm (residuals) and 78 μm (FWHM) with the 50-μm-wide pixels, which will replace the 75-μm ones in the near future. The distributions of centre-of-gravity precision (maximum at 15 μm) and of angular precision (maximum at 8 mrad) of the mini-tracks are plotted in Fig. 15(b) and (c), respectively. The direction precision is particularly important for mini-track extrapolations to the next layer (see track finding and reconstruction algorithm).

With 1024 pixels we did not notice any heat production from the ISPA-anode chip.[7] Each ISPA-pixel covers 0.5 $\times$ 0.05 mm^2 of the fiber end-section. This corresponds to a subtended tracker surface per hit of 0.025 mm$^2\times$ 2500 mm (fiber length)/0.25 mm (hit layer) = 2.5 $\times$ 10^{-4} m^2. This results in 4000 readout channels per 1 m^2 of subtended tracker surface per hit with a corresponding heat production of 100 mW. Even increasing the estimated heat per pixel by four times, this power (0.4 W) would be dissipated without an extra-cooling of the tracker.

[7] F. Anghinolfi *et al.* [24] estimate 25 μW heat per electronic pixel.

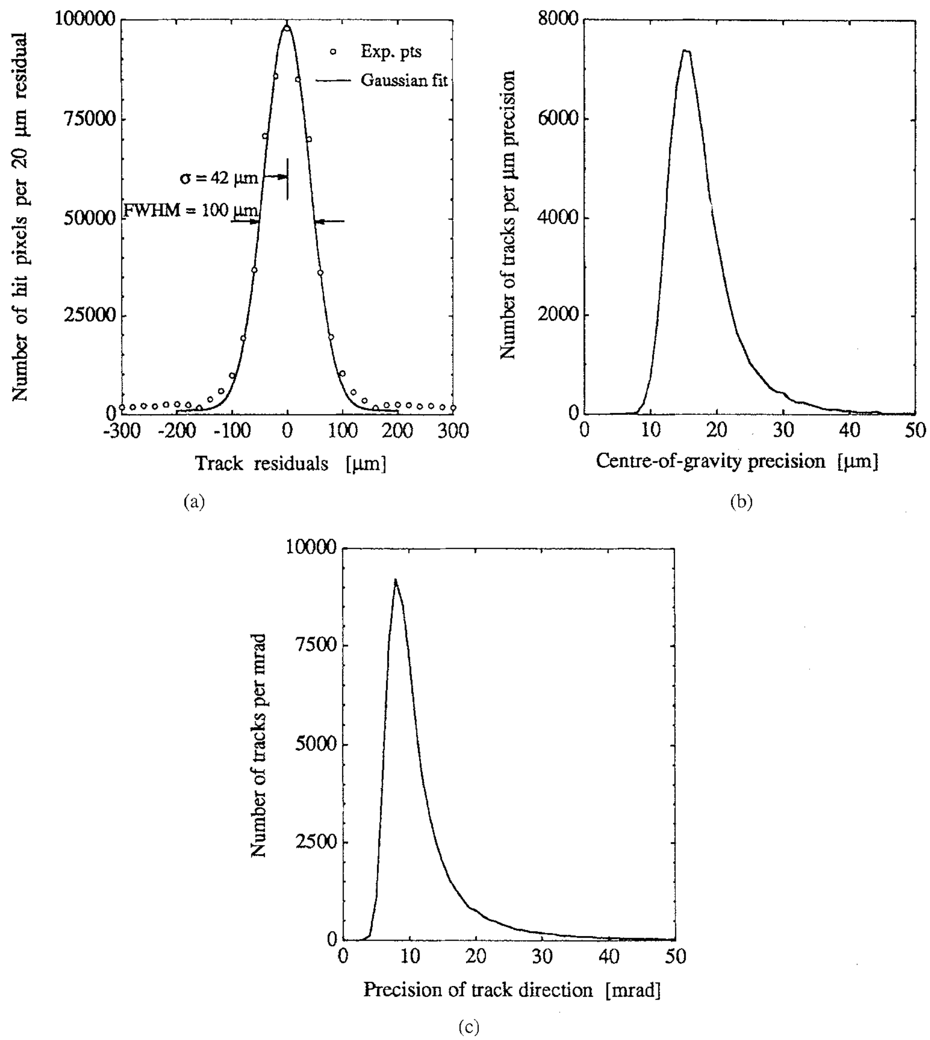

Fig. 15. (a) Residuals from 10^5 pion tracks (circles) and their Gaussian fit. The standard deviation σ and the FWHM value are due to the binary ISPA readout, which disregards the number of hits within 1 pixel. An analog readout would reduce this dominant contribution of the 75 μm pixel widths and therefore improve both values. (b) The center-of-gravity precision ε is related to the number of hit pixels: $\varepsilon = \sigma/\sqrt{N}$. The asymmetric shape is mainly due to the diminishing number N of hit pixels at the right-hand part. (c) Direction precisions of 10^5 pion tracks, i.e., the angular accuracy with which the mini-tracks of an outer layer can be projected to inner layers or tracker shells. It is roughly proportional to $\frac{2\sigma}{L\sqrt{N}}$, where L is the ribbon thickness (7 mm).

H. Tracker Alignment and Mechanical Support

To achieve the required performance of the fiber tracker (residuals of 30 μm) it is of crucial importance to align the scintillating fibers within a tolerance of less than 10 μm. This can be realized by the following procedures.

First, we must verify the parallelism (coherency) of the individual fibers within a fused bundle. Therefore, we photographed through the entire bundle length (see the camera arrangement in [9]) with parallel slits of 10 μm width each at its light entrance face (Fig. 16). These tests were cross-checked by shining a collimated He-Ne laser beam (wavelength 633 nm, to avoid light absorption within the fibers) at different positions transversely through the bundle. The light scattered into the total reflection acceptance of the fibers shows at the endface always the same fiber row illuminated, which confirms their coherency. After many verifications, we proved that the fiber coherency is in fact an inherent property of the bundle production if the standard light transmission (hit density) is achieved.

Each of the tracker shells would be supported by an appropriately dimensioned cylinder of honeycomb-structured carbon fiber epoxy. This material is very stiff and extremely light (density: 0.2 g cm^{-3}) with 45.1 g cm^{-2} radiation length. All support cylinders of 10 mm wall thickness each would add together only 1.3% of radiation length to the mass-layer (6.7% radiation length) of the fiber tracker.

To arrange the fiber bundles appropriately to their respective support cylinders we stretch some 20 to 30 of them side by side in a metallic mould shaped to the corresponding shell curvature. They are secured coherently together by a sheet of 0.5 mm plexiglass (0.13% of radiation length) glued on top of the bundles. In this way, stiff ribbons of 20–30 coherent fiber bundles are obtained that can be consecutively attached to their respective support cylinders.

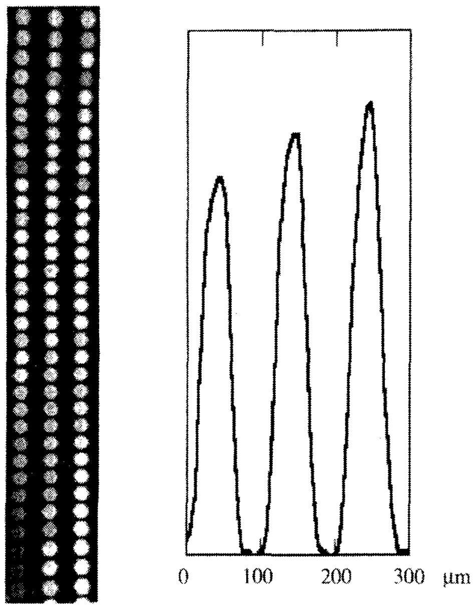

(a) (b)

Fig. 16. (a) A fiber bundle was illuminated uniformly at its entrance face (2.5×2.5 mm^2) through a grid with 10-μm-wide slits and 100-μm pitch. Its exit face was focussed with a telescope onto a CCD camera. (b) The corresponding transverse intensity distribution of the three fiber rows. It is partly affected by the slight mismatch between the grid period (100 μm) and the bundle period (120 μm). The FWHM amounts to 42 μm.

Each of the fiber shell support cylinders is kept in position by thin-walled (5 mm) plexiglass spoke wheels (Fig. 2), which are centerd around the beam pipe of the collider or on the inner- or center-shell. The plexiglass wheels at the extreme ends of the shells ($\eta = \pm 1.5$) carry black fiducial lines (Fig. 17) above their support rims. They appear as nonactivated pixel lines in the ISPA tubes on the other end of the fiber half-shell ($\eta = 0$) (Fig. 18) each time a low-level illumination of the plexiglass wheels is switched on. In this way, the fibers' coherency and their location can be monitored any time during the LHC runs.

IV. Discussion and Conclusion

During our research and development work for particle tracking with scintillating fibers, we have developed a new species of fine grain fibers. In addition, we have introduced a completely new and compact readout technique for their scintillation signals.

First, we replaced the well known two-component dopants, applied in NE- and Bicron-plastic scintillators, by PMP [17], [18], which bridges, due to its large Stokes' shift, the region from 300 nm (absorption peak) to 420 nm (emission peak) without wavelength shifter. This avoids, due to local light emission [20], any cross-talk between neighbored fibers and increases their light transmission by 1.8 times due to well-separated absorption and emission bands of the new dye.

To obtain small diameter fibers in a manipulatable form we developed, in close collaboration with Kuraray Co.,[8] fiber bundles of squares cross section.[9] They contain between several hundred and a few thousand individual fibers fused together (Fig. 4). This new method guarantees the fiber coherency and improves their packing fraction by 1.3 times.

[8] Kuraray Co. Ltd., Methacrylic Division, Tokyo 103, Japan.

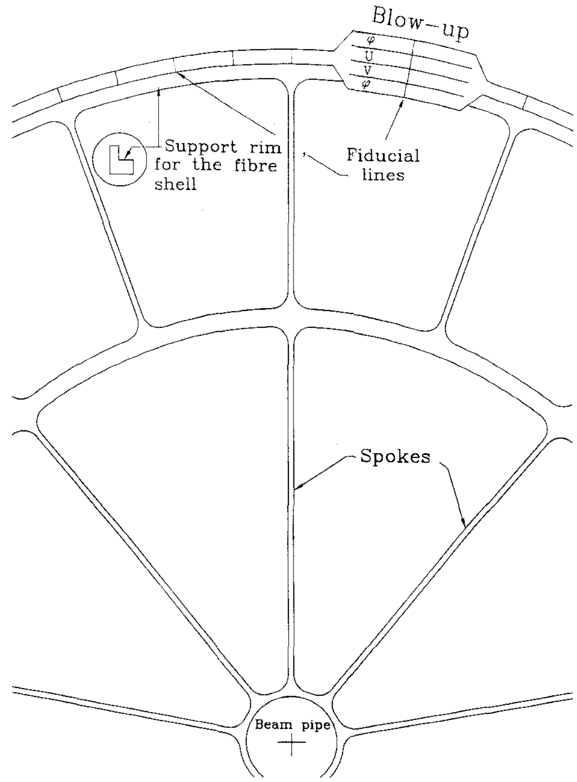

Fig. 17. Example of a plexiglass wheel placed at one of the extreme tracker ends (Fig. 2). It supports one shell end and carries at the same time black fiducial lines. Once scarcely illuminated, they appear as nonactivated pixel rows (Fig. 18) of the ISPA tubes at the ISPA end of the shell.

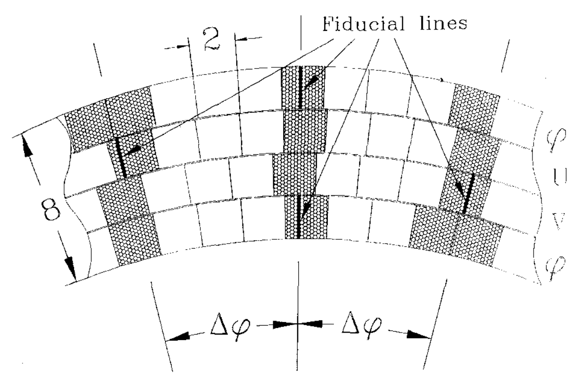

Fig. 18. Example of nonactivated pixel rows due to the illumination of the plexiglass template at the other end of a tracker shell. It marks $\Delta\varphi_{\max} = \tan\alpha \cdot \sinh\eta_{\max}$. With the known stereo angle α, it is possible to control the rapidity $\eta_{\max}$ or the maximum polar angle θ ($\mathrm{cotg}\theta_{\max} = \sinh\eta_{\max}$) covered by the tracker shell in question.

[9] The gap between their sensitive area is 50 μm caused by their PMMA boundaries. This causes 2% (center and outer shell in Fig. 1) or 2.5% (inner shell) dead space for one bundle layer. Two layers reduce it already to 0.04% and so on (Fig. 18). These numbers represent the worst case where all particle tracks are strictly radial at 90° polar angle.

To enhance the light-trapping fraction of the fibers, we introduced a new double-cladding method. Instead of the common PMMA cladding, we proposed to Kuraray Co. in 1989[10] to clad their fibers with a fluorinated cladding of lower refractive index. This is now applied routinely by Kuraray and increases the trapping fraction by 1.8 times.

The readout of fiber signals has been drastically simplified by the development of ISPA tubes [3], [23]. These new and compact position-sensitive light detectors enhance the number of detected photoelectrons by 1.6 times, are gatable, and read out in less than 10 μs while data taking is going on. In this way, they improve the signal-to-noise ratio as compared to the bulky chain of several conventional image intensifiers with their noisy phosphor screens and CCD readout.

All these fiber developments together with better production performance led finally to the comparatively high hit density displayed in Fig. 3. It provides mini-tracks in the three fiber layers (Figs. 13 and 14) rather than single hits. This facilitates track finding in high-multiplicity environments and improves their reconstruction at high-momentum resolution.

In order to compare scintillating fibers with the competing MSGC's [31]–[34] and silicon strips [2], we list some relevant parameters of the three tracking elements in Table III. These values are best estimates of the present state-of-the-art and, for valuable comparisons, they are normalized either to units of 10% radiation length or to units of subtended detector surface and to the material layer thickness required to achieve one hit from the energy loss of a minimum ionizing particle (scintillating fibers: 0.25 mm; MSGC: 2 mm; Si-strips: 0.3 mm).

The spatial precision listed for scintillating fibers represents the standard deviation of a Gaussian-shaped hit distribution [9]. With Si-strips it is either taken as the standard deviation of the centroid strip distribution (analog readout) or as the strip pitch divided by $\sqrt{12}$ (binary readout). For MSGC's the spatial resolution means the accuracy with which the centroids of drift clusters can be located. In addition, the precision of MSGC's is corrected with their detection efficiency. The single strip efficiency of 96% for perpendicular tracks decreases to between 35% and 15% at 30° angular deviation from normal incidence depending on the threshold [35]. This worsens precision and two-track resolution accordingly.

The two-track resolution indicated for scintillating fibers means the classical resolving power in optics for the spatial resolution of two neighboring objects. Therefore, the listed value refers to the FWHM (2.36 σ) of the Gaussian precision distribution [9]. The two-track resolution reported for Si-strips and for tracks of normal incidence in MSGC's do not relate in this classical way to their claimed precisions. Finally, for a 7-mm-thick ribbon of scintillating fibers, the average center-of-gravity precision is 15 μm and the average angular precision is 10 mrad [23].

[10] Three different fluorinated monomers were shipped by us to Kuraray Co. in February 1990. In March 1991 we measured the first fibers with fluorinated cladding, which unexpectedly resulted in a decrease of light transmission. We then proposed to produce double-clad fibers (usual PMMA plus fluorinated cladding), which finally resulted in the expected increase in light transmission (August 1991).

An important difference between fibers and the two other tracking methods is in the arrangement of the electronic readout. Fibers are readout via their end-sections by ISPA tubes. In contrast to that, every silicon-strip or micro-strip of MSGC's must be equipped with its proper electronic channel, which results in the great channel numbers listed in Table III. An additional problem arises from the heat production of these many electronic channels. It necessitates extra cooling provisions that add still more radiation lengths in the tracking volume.

To conclude, the proposed fiber tracker provides mini-tracks and therefore close to 100% reconstruction efficiency. The fiber bundles and their honeycomb support represent only 8% of radiation length. This reduces the level of ghost tracks below 1% and does not therefore disturb the efficiency and energy resolution of the electromagnetic calorimeter. The ISPA readout provides the delay for the first-level trigger and a complete track picture in about 10 μs with the present chip. In the future, it is foreseen to reach readout times of less than 1 μs. Its low heat production obviates any cooling provision.

Acknowledgment

The authors are grateful to P. Destruel (CNRS, Toulouse, France), U. Gensch (DESY, Hamburg, Germany), H. Güsten (Forschungszentrum Karlsruhe, Germany), T. Shimizu (Kuraray Co. Ltd, Tokyo, Japan), E. Barni, and G. Viscardi (University of Torino, Torino, Italy), who provided them with information and helpful discussions. D. Piedigrossi and S. Tailhardat contributed with their technical skills to the experimental arrangements and measurements.

References

[1] CMS, "The compact muon solenoid," Tech. Proposal, CERN/LHCC 94-38.

[2] ATLAS, "Technical proposal for a general-purpose pp experiment at the Large Hadron Collider at CERN," Tech. Proposal, CERN/LHCC 94-43.

[3] T. Gys, C. D'Ambrosio, H. Leutz, D. Piedigrossi, and D. Puertolas, "A new position-sensitive detector based on an imaging silicon pixel array (ISPA-tube)," *Nucl. Instrum. Methods Phys. Res. A*, vol. 355, p. 386, 1995.

[4] C. D'Ambrosio, T. Gys, H. Leutz, D. Piedigrossi, D. Puertolas, S. Tailhardat, T. Shimizu, and O. Shinji, "Further results on photon counting with small diameter scintillating fibers," *Nucl. Instrum. Methods Phys. Res. A*, vol. 345, p. 279, 1994.

[5] C. D'Ambrosio, P. Destruel, M. Garg, U. Gensch, H. Güsten, T. Gys, H. Leutz, A. Menchikov, D. Piedigrossi, D. Puertolas, T. Shimizu, O. Shinji, and S. Tailhardat, "Development of small diameter scintillating fiber detectors for particle tracking," RD7-Summary Rep., CERN/DRDC 94-48, 1994.

[6] C. D'Ambrosio, T. Gys, H. Leutz, D. Piedigrossi, D. Puertolas, and S. Tailhardat, "Photon counting with a hybrid photomultiplier tube (HPMT)," *Nucl. Instrum. Methods Phys. Res. A*, vol. 338, p. 389, 1994.

[7] C. D'Ambrosio, P. Destruel, U. Gensch, H. Güsten, T. Gys, H. Leutz, F. Pengg, D. Piedigrossi, D. Puertolas, S. Schlenstedt, W. Seidl, T. Shimizu, O. Shinji, J. Sun, and S. Tailhardat, "RD7: Central tracking with scintillating fibers," 1991 Status Rep., CERN/DRDC 91-55, 1991.

[8] C. D'Ambrosio, T. Gys, H. Leutz, D. Piedigrossi, D. Puertolas, S. Tailhardat, T. Shimizu, and O. Shinji, "Photoelectron counting with small diameter scintillating fibers," *Nucl. Instrum. Methods Phys. Res. A*, vol. 332, p. 134, 1993.

[9] C. D'Ambrosio, H. Leutz, T. Shimizu, and O. Shinji, "Imaging performance obtained with fused bundles of scintillating fibers," *Nucl. Instrum. Methods Phys. Res. A*, vol. 325, p. 161, 1993.

[10] F. Anselmo, F. Block, L. Cifarelli, C. D'Ambrosio, T. Gys, G. La Commare, H. Leutz, M. Marino, and S. Qian, "Track reconstruction

with a central two-shell scintillating fiber tracker (SFT)," *Nucl. Instrum. Methods Phys. Res. A*, vol. 349, p. 398, 1994.

[11] R. L. Gluckstern, "Uncertainties in track momentum and direction due to multiple scattering and measurements errors," *Nucl. Instrum. Methods Phys. Res.*, vol. 24, p. 381, 1963.

[12] C. D'Ambrosio, T. Gys, H. Leutz, U. Gensh, and S. Schlenstedt, "Optimization of central particle tracking at future hadron colliders," *Nucl. Instrum. Methods Phys. Res. A*, vol. 322, p. 20, 1992.

[13] ——, "Central tracking in high luminosity future colliders," in *Supercolliders and Superdetectors, Proc. 25th Workshop INFN Eloisatron Project*, W. A. Barletta and H. Leutz Eds., Erice, Italy, Nov. 1992.

[14] C. D'Ambrosio and S. Qian, "Monte Carlo simulation for the scintillating fibers tracking detector and its resolution evaluation," *Nucl. Instrum Methods Phys. Res. A*, vol. 335, p. 341, 1993.

[15] R. Brun, F. Bruyant, M. Maire, A. C. McPherson, and P. Zanarini, "GEANT 3," CERN/DD/EE/84-1, 1987.

[16] P. Billoir and S. Qian, "Simultaneous pattern recognition and track fitting by the Kalman filtering method," *Nucl. Instrum. Methods Phys. Res. A*, vol. 294, p. 219, 1990.

[17] H. Güsten, P. Schuster, and W. Seitz, "Organic scintillators with unusually large Stokes shifts," *J. Phys. Chem.*, vol. 82, p. 459, 1978.

[18] C. D'Ambrosio, H. Leutz, M. Taufer, and H. Güsten, "New organic scintillators with large Stokes shifts," *Appl. Spectrosc.*, vol. 45, p. 484, 1991.

[19] H. Leutz, "Scintillating fibers," *Nucl. Instrum. Methods Phys. Res. A*, vol. 364, p. 422, 1995.

[20] T. Förster, "Zwischenmolekulare energiewanderung und fluoreszenz," *Ann. Phys.*, vol. 2, p. 55, 1948.

[21] D. E. Groom, "Radiation at hadron collider: Scaling to the highest energies," in *Supercolliders and Superdetectors, Proc. 25th Workshop of the INFN Eloisatron Project*, W. A. Barletta and H. Leutz, Eds., Erice, Italy, Nov. 1992.

[22] C. D'Ambrosio, P. Destruel, M. Garg, U. Gensch, H. Güsten, T. Gys, H. Leutz, D. Piedigrossi, D. Puertolas, T. Shimizu, O. Shinji, and S. Tailhardat, "RD7: Central tracking with scintillating fibers," 1993 Status Rep., CERN/DRDC 93-42, Oct. 1993.

[23] C. D'Ambrosio, T. Gys, H. Leutz, D. Piedigrossi, and D. Puertolas, "First beam exposures of a scintillating fiber tracker read out by an ISPA-tube," *Nucl. Instrum. Methods Phys. Res. A*, vol. 359, p. 618, 1995.

[24] F. Anghinolfi *et al.*, "A 1006 element hybrid silicon pixel detector with strobed binary output," *IEEE Trans. Nucl. Sci.*, vol. 39, p. 654, 1992.

[25] E. H. M. Heijne *et al.*, "First operation of a 72 k element hybrid silicon micropattern pixel detector array," *Nucl. Instrum. Methods Phys. Res. A*, vol. 349, p. 138, 1994.

[26] S. Aoki *et al.*, "Scintillating fiber trackers with optoelectronic readout for the CHORUS neutrino experiment," *Nucl. Instrum. Methods Phys. Res. A*, vol. 344, p. 143, 1994.

[27] R. E. Ansorge *et al.*, "Performance of a scintillating fiber detector for the UA2 upgrade," *Nucl. Instrum. Methods Phys. Res. A*, vol. 265, p. 33, 1988.

[28] M. Atac, J. Park, D. Cline, D. Chrisman, M. Petroff, and E. Anderson, "Scintillating fiber tracking for the SSC using Visible Light Photon Counters," *Nucl. Instrum. Methods Phys. Res. A*, vol. 314, p. 56, 1992.

[29] B. Baumbaugh *et al.*, "Performance of multiclad scintillating and clear waveguide fibers read out with visible light photon counters," *Nucl. Instrum. Methods Phys. Res. A*, vol. 345, p. 271, 1994.

[30] M. Adams, N. Amos, D. A. Averill, P. Baringer, M. Chung, F. Hsieh, H. Li, D. Lincoln, S. Margulies, H. Neal, E. Neis, L. Oesch, J. Qian, M. Rijssenbeek, and T. Yasuda, "A detailed study of plastic scintillating strips with axial wavelength shifting fiber and VLPC readout," *Nucl. Instrum. Methods Phys. Res. A*, vol. 366, p. 263, 1995.

[31] A. Oed, "Position sensitive detector with microstrip anode for electron multiplication with gases," *Nucl. Instrum. Methods Phys. Res. A*, vol. 263, p. 351, 1988.

[32] F. Angelini, R. Bellazini, A. Brez, M. M. Massai, G. Spandre, and M. R. Torquati, "A microstrip gas avalanche chamber with two-dimensional readout," *Nucl. Instrum. Methods Phys. Res. A*, vol. 283, p. 755, 1989.

[33] F. Udo, "Application of the microstrip gascounter in a LHC tracker," in *Proc. Large Hadron Collider Workshop*, G. Jarlskog and D. Rein, Eds., CERN 90-10, 1990, vol. 3, p. 219.

[34] F. Angelini, R. Bellazini, A. Brez, M. M. Massai, G. Spandre, and M. R. Torquati, "The microstrip gas chamber," *Nucl. Phys. B (Proc. Suppl.)*, vol. A23, p. 254, 1991.

[35] "Development of gas microstrip chambers for radiation detection and tracking at high rates," RD-28 collaboration, CERN/DRDC 93-34, 1993.